Sains Malaysiana 47(2)(2018): 253-259
http://dx.doi.org/10.17576/jsm-2018-4702-06

Cr_2O_3 Nanoparticles Anchored on ZnO Nanorods as Active Heterostructure Catalysts for Phenol Degradation

(Zarah Nano Cr_2O_3 Bergabung pada Rod Nano ZnO sebagai Pemangkin Heterostruktur Aktif untuk Degradasi Fenol)

SZE-MUN LAM*, JIN-CHUNG SIN & ABDUL RAHMAN MOHAMED

ABSTRACT

With the rapid civilization and industrialization, water pollution is becoming more and more intricate. Heterogeneous photocatalysis using metal oxide loaded ZnO nanorods is a well-known environmental technology to degrade toxic organic pollutants. In this study, Cr_2O_3 particles anchored on the ZnO nanorods (Cr_2O_3/ZnO) were successfully synthesized by a hydrothermal-deposition technique. Microscopic and crystallographic analyses indicated that the synthesized samples consisted of two-phase heterostructure of Cr_2O_3 and ZnO. The photocatalytic results showed that the phenol degradation by Cr_2O_3 /ZnO heterostructures was higher than those of pure ZnO and commercial TiO_2. The synergetic effect between Cr_2O_3 and ZnO was the pivotal reason for the improvement of photoactivity as proven by the photoluminescence and terephthalic acid–photoluminescence analyses.

Keywords: Cr_2O_3; nanocomposite; phenol; photocatalysis; ZnO nanorod

ABSTRAK

Dengan pertamadunan dan perindustrian yang pesat, isu alam sekitar seperti pencemaran air menjadi semakin rumit. Fotopemangkinan heterogen menggunakan logam oksida digabungkan rod nano ZnO adalah teknologi alam sekitar yang terkenal untuk degradasi bahan pencemar organik toksik. Dalam kajian ini, heterostruktur Cr_2O_3/ZnO dengan zarah Cr_2O_3 berpasang pada rod nano ZnO telah berjaya disintesis oleh teknik hidroterma-pemendapan. Analisis mikroskopik dan kristalografi menunjukkan bahawa sampel yang disintesis terdiri daripada dua fasa berheterostruktur Cr_2O_3 dan ZnO. Keputusan fotopemangkinan menunjukkan bahawa degradasi fenol oleh heterostruktur Cr_2O_3/ZnO adalah lebih tinggi berbanding dengan ZnO tulen dan TiO_2 komersial. Kesan sinergi di antara Cr_2O_3 dan ZnO adalah sebab utama peningkatan aktiviti pemfotomangkinan seperti yang dibuktikan oleh analisa fotoluminasi dan asid tereftalik-fotoluminasi.

Kata kunci: Cr_2O_3; fenol; fotopemangkinan; komposit nano; rod nano ZnO

INTRODUCTION

Heterogeneous photocatalysis using semiconductors for water and wastewater treatment continues to garner prime attention. The low cost of catalysts, ease of operation feasibility and the environmental security make this technique very exceptional in comparison to other methods. The basic principle of this process is according to the photoactivation of catalysts, the efficacy is affected by the capability to form charge carrier and followed by active radical formation. Hence, the selection of suitable catalysts is pivotal to the reactivity control. ZnO is a wide direct band gap (~3.3 eV) semiconductor which has recognized to be a serious candidate whose physico-chemical attributes are analogous to those of TiO_2 (Khalik et al. 2015; Lee et al. 2014). However, the photoactivity of ZnO was limited by the rapid recombination of the charge carrier (Sin et al. 2013). To overcome this bottleneck, two major solutions were proposed: the first method was to improve the specific surface area and it can be achieved by preparing ZnO nanostructures with different morphologies. A myriad of unique morphologies of ZnO including rods, tubes, wires, spheres and flowers (Sin et al. 2014; Wang et al. 2009) have been recently fabricated. Meanwhile, researchers also observed that ZnO-based heterojunctions by coupling with other semiconductors (WO_3, Nb_2O_5, CuO) (Cao et al. 2011; Lam et al. 2014; Yang et al. 2014) or depositing noble metals (Au, Ag, Pt) (Flores et al. 2011; Thongsuriwong et al. 2012; Wang et al. 2009) could efficiently improve the photocatalytic activity.

Cr_2O_3 is a wide band gap (~3.4 eV) semiconductor and shows high electrical conductivity as well as high thermal and chemical stability (Li et al. 2014; Su et al. 2014). It is utilized industry as a refractory, high temperature oxidation resistance materials and catalysts (Li et al. 2014). Earlier report on the fabrication of TiO_2 coupled with Cr_2O_3 and its photodegradation applications in presence of UV light irradiation have been revealed (Jung et al. 2011; Zhang et al. 2009). Nevertheless, there is scare report on the coupling of ZnO with Cr_2O_3 (Xia et al. 2015). In Cr_2O_3 coupled ZnO catalysts, the Cr_2O_3 conduction band (CB) was higher than that of ZnO. Under

exposure to UV light, Cr_2O_3 could be photoexcited and the photogenerated electrons (e^-) could be transferred into the CB of ZnO due to the CB states of ZnO was lower than that of Cr_2O_3. Thus, the movement of e^- efficiently promoted the separation between the photogenerated e^- and holes (h^+) as well as decreased the chance of light-induced corrosion on ZnO photocatalysts.

Phenol is extensively utilized as a monomer for the production of resins, wood, fertilizers, explosives, plastic plasticizers, lubricants, rubbers and textiles (Busca et al. 2008). In Malaysia, the phenol concentration ranging from 0.8–53.6 µg/L have been identified from the effluents of timber sawmills, rubber processing factories, motor and battery workshops, engineering workshops as well as animal farming and agricultural activities (Abdullah & Nainggolan 1990). For example in the Seremban municipality, the phenol levels in the Linggi River exceeded the permitted Malaysian standard of 2.0 µg/L for raw water (Abdullah & Nainggolan 1990). Since phenol is termed as toxic and recalcitrant pollutant (Busca et al. 2008; Patniak et al. 2007), heterogeneous photocatalysis which can bring a complete mineralization of the organic pollutant is well matched for this work.

Hence, the present study emphasizes on the preparation of Cr_2O_3 coupled with ZnO nanorods via a hydrothermal-deposition route for the photodegradation of phenol under UV light. Based on above the consideration, it was anticipated that Cr_2O_3/ZnO heterostructures have the potential to circumvent the ZnO photocorrosion because of their special structures and different interfacial potentials, which allowed the e^- transportation from ZnO nanorods and Cr_2O_3 to absorbate species. It was also worth mentioning that the improved photocatalytic mechanism of Cr_2O_3/ZnO heterostructures was elucidated.

Materials and Methods

In a typical experiment, pure ZnO nanorods were prepared through hydrothermal route according to our previous study (Lam et al. 2014). Cr_2O_3/ZnO nanorods were fabricated through a chemical-deposition method as follows: 1.0 g of pure ZnO nanorods was ultrasonicated for 30 min in 50 mL deionized water (DI) and ammonia solution was then added drop-by-drop into the solution. Subsequently, 0.6 mmol $Cr(NO_3)_3 \cdot 9H_2O$ was dissolved into above mixtures and followed by stirring for 12 h. After that, the as-produced precipitates were filtered, washed with distilled water, dried at 60°C for 12 h and finally calcined at 400°C for 2 h. For a comparison, pure ZnO nanorods were also calcined at 400°C for 2 h.

The as-prepared samples were characterized by field emission-scanning electron microscopy (FESEM) using a Quanta FEG 450 coupled with an energy dispersive X-ray (EDX). The transmission electron microscopy (TEM) image was taken using a Philips CM-12 operated at 120 keV. The high resolution transmission electron microscopy (HRTEM) image was captured using a Fei Tecnai 20. X-ray diffraction (XRD) analysis was carried out using a Philips PW1820 diffractometer equipped with Cu Kα radiation at 40 kV and 120 mA. The samples were scanned in the 2θ ranging from 20° to 80° at scanning rate of 0.03° per second. UV–vis diffuse reflectance spectroscopy (DRS) spectrum was recorded on a Perkin Elmer Lambda 35 UV-vis spectrophotometer with $BaSO_4$ as a reference. The photoluminescence (PL) analysis was tested using a Perkin Elmer Lambda S55 spectrofluorometer with a Xe lamp excitation wavelength of 325 nm at room temperature.

The photoactivity of the as-prepared Cr_2O_3/ZnO heterostructure was examined using phenol as a model substrate. A batch-mode immersion well reactor was used as a photoreactor for the photocatalytic test. The photoreactor was made of Pyrex glass with dimensions of 200 × 100 × 60 mm (height × outer diameter × inner diameter). A 15 W UV Pen-ray (UVP, Inc.) lamp with a maximum emission at about 365 nm was used as UV source positioned in the center of cylindrical photoreactor. The average UV output intensity at 10 mm away from UV light determined by a radiometer (Cole Parmer, Series 9811) was 1.060 mW/cm^2. In a typical experiment, appropriate amount of catalyst was added to the photoreactor containing 350 mL of 20 mg/L phenol solution. The mixture was equilibrated for 1 h in the dark and followed by the UV irradiation. The heterogeneous mixture was magnetic stirred and bubbled with air at a fixed flow rate of 4 mL/min during the experiment. At specific time intervals, 2 mL of the sample was withdrawn from the system, centrifuged and then the sample concentration was measured by a high performance liquid chromatography (HPLC, Perkin Elmer Series 200). HPLC equipped with an isocratic gradient pump, a 20 µL injection circuit and a variable wavelength UV detector. C18 column (150 mm-length × 4.6 mm-inner diameter × 5 µm-particle size) was used in the sample analysis with mobile phase mixture of water 60% (v/v) and acetonitrile 40% (v/v) at a flow rate of 1 mL/min. The wavelength of detector was set at 238 nm. The photocatalytic procedures were detailed in our previous report (Lam et al. 2013). At the same time, comparison study was made using commercially available TiO_2 Degussa P25 (75% anatase and 25% rutile).

The analysis of hydroxyl radicals (•OH) formation on the sample under UV irradiation was performed using terephthalic acid with photoluminescence (TA–PL) techniques. Experimental methods were same as the photoactivity test except that phenol solution was replaced by the 5×10^{-4} M TA aqueous solution with a concentration of 2×10^{-3} M NaOH solution.

Results and Discussion

The morphology of the as-synthesized ZnO nanorods was captured by FESEM in Figure 1(a). It can be observed that the samples were rod-like nanostructures and grown in large quantity. The typical sizes of nanorods were measured to be 600–800 nm long and 15–25 nm diameter. With the mixed solution of chromium (III) nitrate nanohydrate and ammonium solution, Cr ions

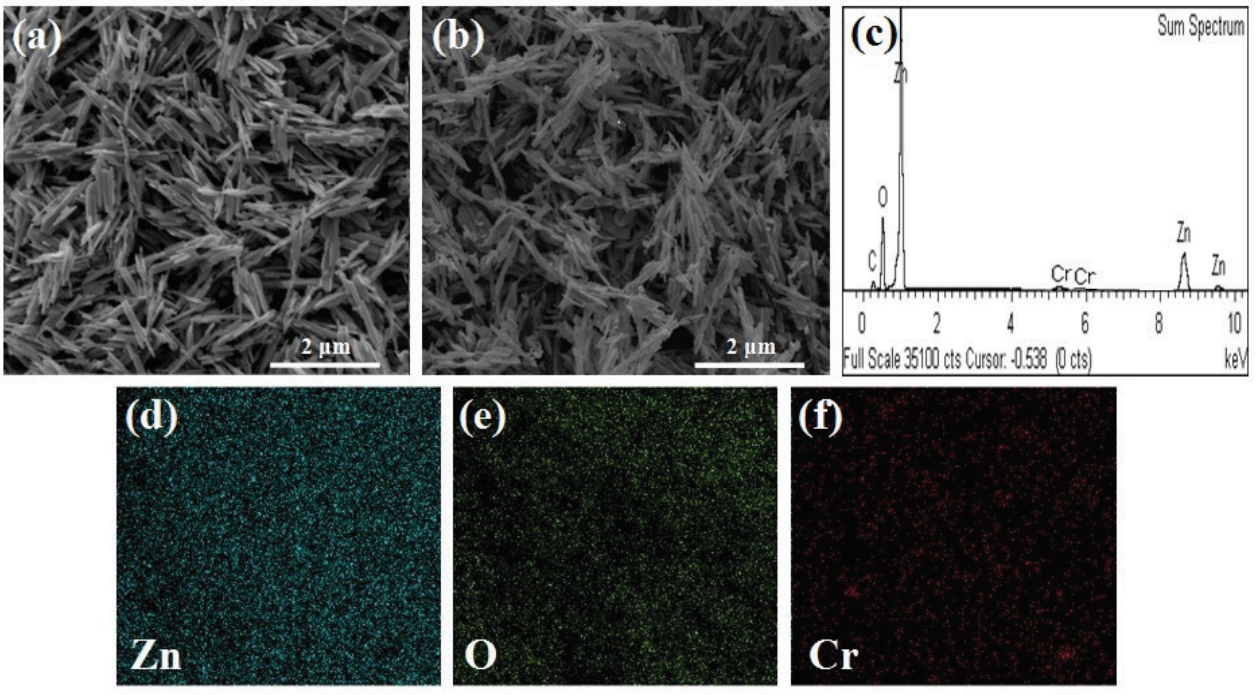

FIGURE 1. FESEM images of (a) pure ZnO (b) Cr_2O_3/ZnO heterostructures (c) The EDX spectrum of Cr_2O_3/ZnO heterostructures and (d–f) elemental mapping images of Cr_2O_3/ZnO heterostructures

were homogeneously dispersed on the ZnO nanorod surfaces. These Cr ions were hypothesized to nucleate from the defect sites of the ZnO nanorods and grew up. The subsequent calcination at 400°C for 2 h made the Cr ions became Cr_2O_3 without altering the morphology of the Cr_2O_3 nanoparticles. The FESEM image Cr_2O_3/ZnO heterostructures is displayed in Figure 1(b). It can be found that the Cr_2O_3/ZnO nanorods consisted of small Cr_2O_3 nanoparticles attached on the ZnO nanorod surfaces. The elemental analysis of Cr_2O_3/ZnO heterostructures was identified using the EDX (Figure 1(c)). The Zn, O and Cr peaks can be obviously found. The weak C peak was also detected, which came from the supporting carbon tape. Furthermore, the EDX mapping of Cr_2O_3/ZnO heterostructures in Figure 1(d)–1(f) indicated that Zn, O and Cr ions were uniformly dispersed in the samples.

TEM image shown in the Figure 2(a) showed that the Cr_2O_3/ZnO heterostructures were comprised of two distinct phases. The spherical-shaped particles were Cr_2O_3 with particle sizes 20 to 50 nm. It was noticeable that the Cr_2O_3 nanoparticles were randomly distributed on the ZnO nanorods and formed heterostructures. To further confirm the microstructure of the Cr_2O_3/ZnO heterostructures, HRTEM analysis was conducted. The HRTEM image of Cr_2O_3/ZnO heterostructures in Figure 2(b) shows two distinct sets of lattice fringes corresponding to the (002) plane of hexagonal phase ZnO and the (012) plane of hexagonal phase Cr_2O_3. From the TEM and HRTEM images, it can be observed that the Cr_2O_3/ZnO heterostructures have highly crystalline structure, which was pivotal for excellent photocatalytic materials.

XRD patterns of pure ZnO and Cr_2O_3/ZnO heterostructures are shown in Figure 3(a). The diffraction

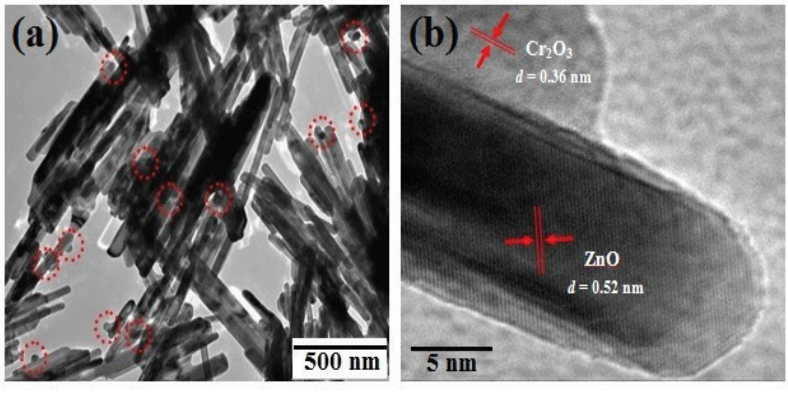

FIGURE 2 (a) TEM image of Cr_2O_3/ZnO heterostructures (recorded from red dot circle was Cr_2O_3 nanoparticles) and (b) HRTEM image of Cr_2O_3/ZnO heterostructures

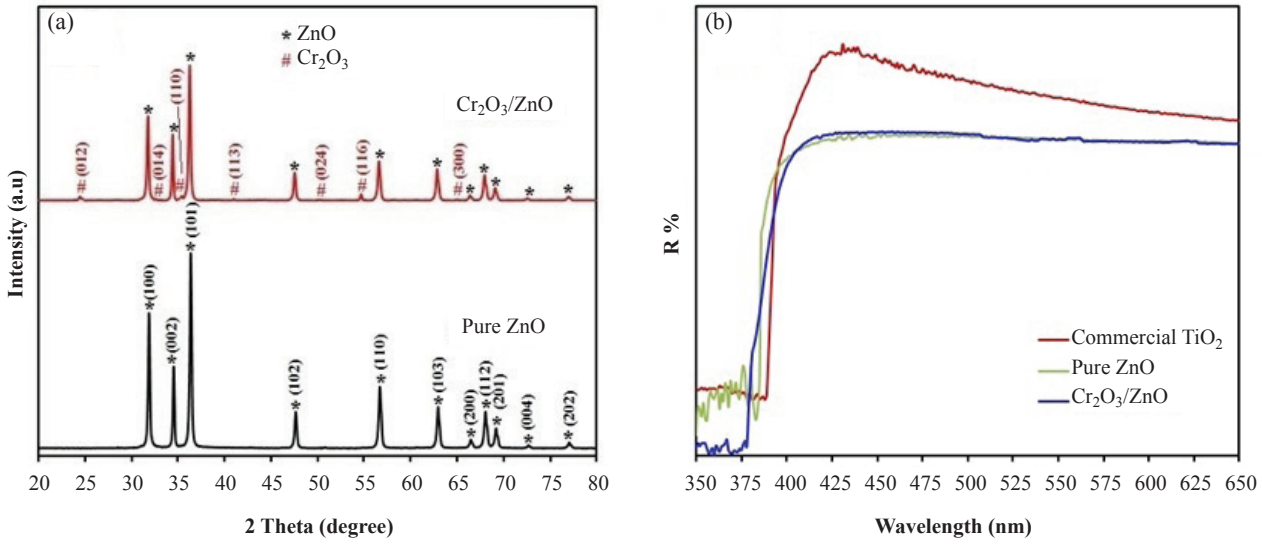

FIGURE 3 (a) XRD patterns and (b) UV-vis DRS spectra of pure ZnO and Cr_2O_3/ZnO heterostructures

peaks of pure ZnO can be assigned to the hexagonal wurtzite phase ZnO (JCPDS Card No. 36-1451). After the introduction of Cr_2O_3, hexagonal phase Cr_2O_3 (JCPDS Card No. 38-1479) which labeled as "#" was found in the Cr_2O_3/ZnO heterostructures. This indicated that the as-prepared Cr_2O_3/ZnO composed of two-phase structure of hexagonal wurtzite ZnO and hexagonal phase Cr_2O_3. Meanwhile, all peaks of XRD patterns were narrow because of high crystallinity and no peaks belonging to any impurities were found. Figure 3(b) shows the UV–Vis DRS spectra of the as-synthesized samples. It was noticeable that the light absorption of the Cr_2O_3/ZnO heterostructures in the UV light region was higher than those of pure ZnO and commercial TiO_2, suggesting their potential UV photocatalytic activity. The band gap energies of pure ZnO, commercial TiO_2 and Cr_2O_3/ZnO heterostructures were calculated to be 3.24, 3.20 and 3.31 eV, respectively.

Photoluminescence (PL) was used to give some information relating to the separation and recombination behaviour of charge carriers in a typical semiconductor. Figure 4 exhibits the PL emission spectra of the as-synthesized samples at excitation wavelength 325 nm. It can be seen that the position and pattern of the emission peaks of all samples were almost similar, but the PL intensities of the samples were markedly different. Especially, the PL pattern of the Cr_2O_3/ZnO heterostructures displayed significant reduction in emission yield in comparison to that of pure ZnO. Such a reduction in emission could be ascribed to the effective charge injection process between the Cr_2O_3 nanoparticles and ZnO nanorods. Several researchers have stated that since the PL signal was the result of the charge carrier recombination, the lower PL intensity indicated a lower charge carrier recombination rate and corresponded to higher photoactivity (Liu et al. 2013; Sin et al. 2014; Su et al. 2011). The results showed that Cr_2O_3/ZnO heterostructures have lower charge carrier recombination rate, demonstrating that the charge carriers have longer

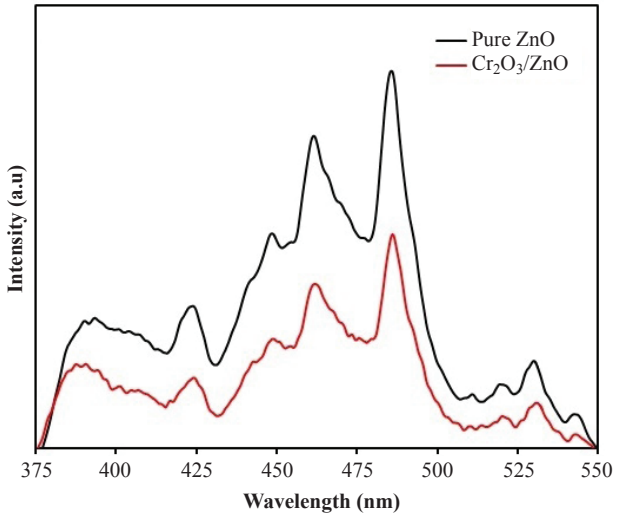

FIGURE 4. PL spectra of pure ZnO and Cr_2O_3/ZnO heterostructures

lifetime and might produce more reactive species partook in the photocatalytic reaction.

The photoactivities of pure ZnO, commercial TiO_2 and Cr_2O_3/ZnO heterostructures were examined by the phenol solution degradation in the presence of UV light. The results showed that the degradation of phenol without catalyst was negligible under exposure of UV light. Figure 5(a) shows a complete degradation of phenol was attained by Cr_2O_3/ZnO heterostructures within 90 min. The degradation rate achieved the maximum value of 0.0611 min^{-1}, which was 4.9 and 5.6 times higher than those of the pure ZnO and commercial TiO_2, correspondingly (Figure 5(b)). The results implied that the as-synthesized Cr_2O_3/ZnO heterostructures displayed high UV photoactivity for phenol degradation.

A possible mechanism was proposed to elucidate the enhancement of the photocatalytic behaviours of the Cr_2O_3/ZnO heterostructures. Under UV irradiation, both semiconductors were excited. The e^- in valence band (VB)

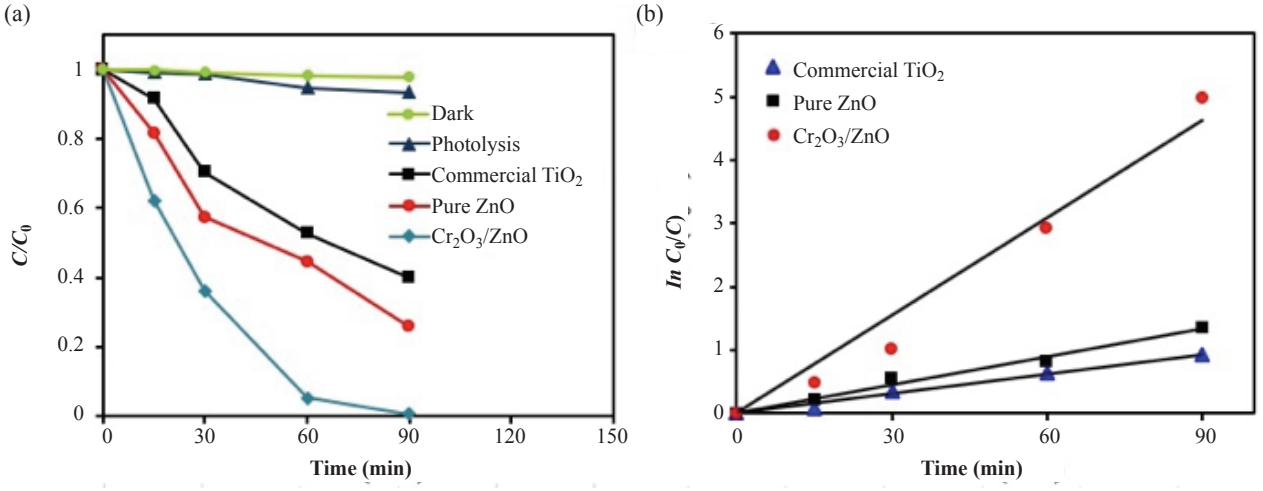

FIGURE 5. (a) Degradation results of phenol solution under different conditions and (b) kinetics plot for the photodegradation of phenol using different catalysts

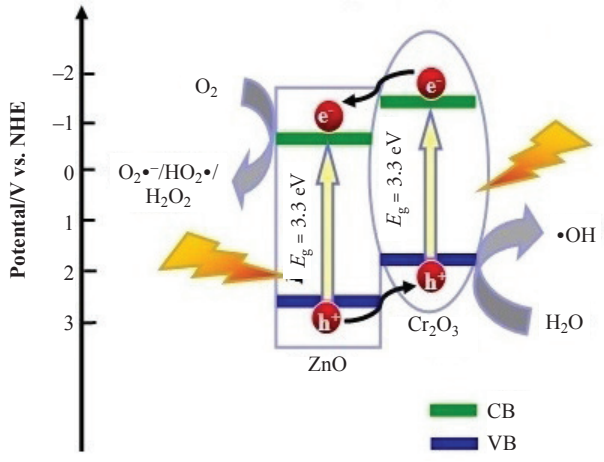

FIGURE 6. Schematic diagram of photogenerated e^-–h^+ separation and transport for the Cr_2O_3/ZnO heterostructures

would be excited to CB for each of them, then e^- in the CB of Cr_2O_3 would be shuttled to the CB of ZnO because the CB of Cr_2O_3 (–1.5eV (Greiner et al. 2011)) was higher than that of ZnO (–0.5 eV (Liu et al. 2013)) and h^+ in the VB of ZnO (2.8 eV (Liu et al. 2013)) would transport to the VB of Cr_2O_3 (2.0 eV (Greiner et al. 2011)) as the former was lower than the latter, thus hindering the e^-–h^+ recombination. After separation, h^+ accumulated in the VB of Cr_2O_3 would react with H_2O in the reaction system to form •OH radicals which have strong oxidizing ability for phenol degradation. The e^- accumulated in the CB of ZnO would react with O_2 to generate superoxide (O_2•$^-$) radicals, hydroperoxyl (HO_2•) radicals and hydrogen peroxide (H_2O_2). These radicals and H_2O_2 would eventually convert to •OH radicals to degrade phenol efficiently as well (Lam et al. 2014; Li et al. 2014). The schematic diagram of this process is shown in Figure 6.

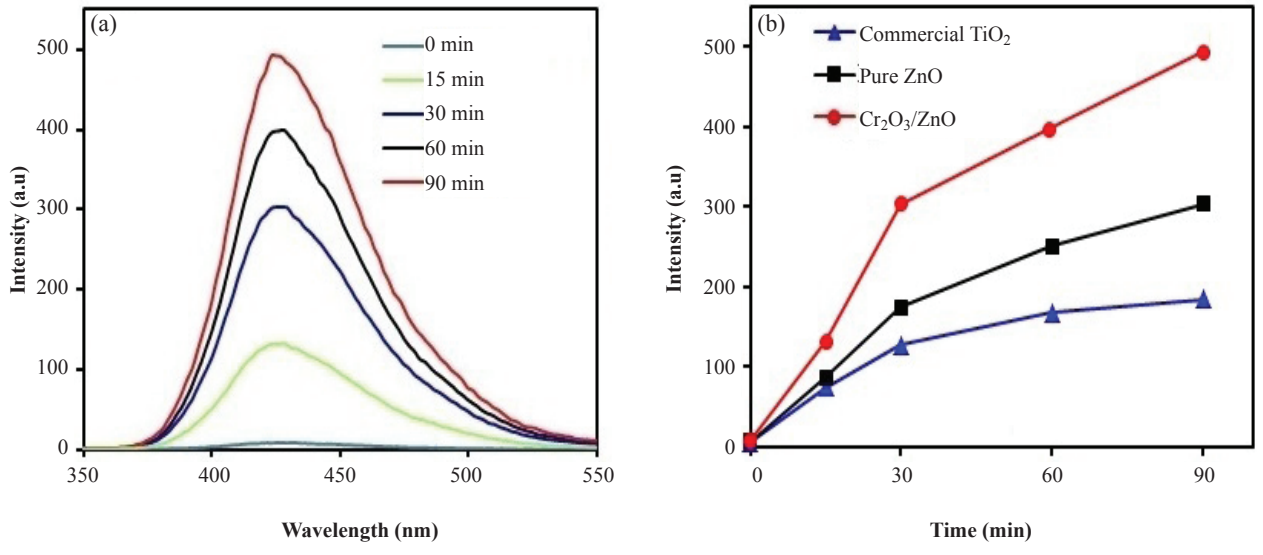

FIGURE 7. (a) TA-PL spectra changes observed during irradiation of the Cr_2O_3/ZnO heterostructures and (b) Plot of the induced PL intensity at 425 nm against irradiation time for TA on different catalysts

To detail the charge carrier transportation at the Cr_2O_3/ZnO heterostructures interface (as shown in Figure 4), TA–PL analysis was carried out to identify •OH radicals produced on the catalysts. As displayed in Figure 7(a), a gradual increase in the PL intensity at about 425 nm was found with increasing irradiation time. The results suggested the fluorescent products, 2-hydroxyterephthalic acid formed during Cr_2O_3/ZnO photocatalysis were due to the chemical reactions of •OH radicals and TA (Cao et al. 2011; Sin et al. 2014). The change of PL spectra with irradiation time for different samples is shown in Figure 7(b). The order of the formation rate of •OH radicals was found to be Cr_2O_3/ZnO > pure ZnO > commercial TiO_2, which inferred that the Cr_2O_3/ZnO heterostructures enhanced the formation rate of •OH radicals. Thus, in this study, Cr_2O_3/ZnO heterostructures could be efficiently prevented the recombination of charge carriers and improved the yield of •OH radicals on the phenol degradation, which further enhanced the Cr_2O_3/ZnO heterostructures photoactivities.

Conclusion

Cr_2O_3/ZnO heterostructures with high UV photoactivity were synthesized by a hydrothermal-deposition technique. The addition of Cr_2O_3 affected the textural and surface characteristics of ZnO nanorods. The Cr_2O_3/ZnO heterostructures exhibited the highest photoactivity with a degradation rate of 0.0611 min^{-1}, which was 4.9 and 5.6 times higher than those of pure ZnO and commercial TiO_2, respectively. The photoactivity improvement of the Cr_2O_3/ZnO heterostructures was due to the high e^-–h^+ pair separation stemming from a good interface connection between two semiconductors with appropriate band structures. This supposition was proven by the PL and TA–PL experiments. This study demonstrated that Cr_2O_3/ZnO was a promising and inexpensive photocatalyst with high photocatalytic activity for organic pollutants degradation.

Acknowledgements

This work was supported by the Universiti Tunku Abdul Rahman (UTARRF/2016–C2/S03 and UTARRF/2017–C1/L02) and Ministry of Higher Education of Malaysia (FRGS/1/2015/TK02/UTAR/02/2 and FRGS/1/2016/TK02/UTAR/02/1).

References

Abdullah, M.D.P. & Nainggolan, H. 1990. Phenolic water pollutants in a Malaysian river basin. *Environmental Monitoring and Assessment* 19: 423–431.

Busca, G., Berardinelli, S., Resini, C. & Arrighi, L. 2008. Technologies for the removal of phenol from fluid streams: A short review of recent developments. *Journal Hazardous Materials* 160: 265–288.

Cao, J., Luo, B.D., Lin H.L. & Chen, S.F. 2011. Photocatalytic activity of novel AgBr/WO_3 composite photocatalyst under visible light irradiation for methyl orange degradation. *Journal Hazardous Materials* 190: 700–706.

Flores, N.M., Pal, U. & Mora, E.S. 2011. Photocatalytic behavior of ZnO and Pt-incorporated ZnO nanoparticles in phenol degradation. *Applied Catalysis A: General* 394: 269–275.

Jung, Y.S., Kim, K.H., Jang, T.Y., Tak, Y.S. & Baeck, S.H. 2011. Enhancement of photocatalytic properties of Cr_2O_3-TiO_2 mixed oxides prepared by sol-gel method. *Current Applied Physics* 11: 358-361.

Khalik, W.F., Ho, L.N., Ong, S.A., Wong, Y.S., Yusoff, N.A. & Ridwan, F. 2015. Decolorization and mineralization of *Batik* wastewater through solar photocatalytic process. *Sains Malaysiana* 44(4): 607–612.

Lam, S.M., Sin, J.C., Abdullah, A.Z. & Mohamed, A.R. 2013. Photocatalytic degradation of resorcinol, an endocrine disrupter, by TiO_2 and ZnO suspensions. *Environmental Technology* 34: 1097–1106.

Lam, S.M., Sin, J.C., Satoshi, I. & Mohamed, A.R. 2014. Enhanced sunlight photocatalytic performance over Nb_2O_5/ZnO nanorod composites and the mechanism study. *Applied Catalysis A: General* 471: 126–135.

Lee, K.M., Abdullah, A.H., Hussein, M.Z. & Zainal, Z. 2014. Synthesis and photocatalysis of ZnO/γFe_2O_3 nanocomposite in degrading herbicide 2,4-dichlorophenoxyacetic acid. *Sains Malaysiana* 43(3): 437–441.

Li, X.Q., Zhang, J., Kang, S.Z., Li, G.D. & Mu, J. 2014. Visible light photocatalytic activity of CuO/Cr_2O_3 co-loaded multiwalled carbon nanotubes sensitized with eosin Y for hydrogen evolution from water. *Ceramics International* 40: 10171–10176.

Liu, W., Wang, M.L., Xu, C.X., Chen, S.F. & Fu, X.L. 2013. Significantly enhanced visible-light photocatalytic activity of g-C_3N_4 via ZnO modification and the mechanism study. *Journal Molecular Catalysis A: Chemical* 368–369: 9–15.

Patniak, P. 2007. *A Comprehensive Guide to the Hazardous Properties of Chemical Substances*. 3rd ed. New Jersey: John Wiley & Sons.

Sin, J.C., Lam, S.M., Satoshi, I. & Mohamed, A.R. 2014. Sunlight photocatalytic activity enhancement and mechanism of novel europium-doped ZnO hierarchical micro/nanospheres for degradation of phenol. *Applied Catalysis B: Environmental* 148: 258–268.

Sin, J.C., Lam, S.M., Lee, K.T. & Mohamed, A.R. 2013. Self-assembly fabrication of ZnO hierarchical micro/nanospheres for enhanced photocatalytic degradation of endocrine-disrupting chemicals. *Material Science in Semiconductor Processing* 16: 1542–1550.

Su, C.Y., Shao, C.L. & Liu, Y.C. 2011. Electrospun nanofibers of TiO_2/CdS heteroarchitectures with enhanced photocatalytic activity by visible light. *Journal of Colloid Interface Science* 359: 220–227.

Su, J.L., Xuen, H.S., Gu, M., Xia, H. & Pan, F.S. 2014. Synthesis of spherical Cr_2O_3 nanoparticles by a microwave refluxing method and their photocatalytic properties. *Ceramics International* 40: 15051–15055.

Thongsuriwong, K.P., Amornpitoksuk, P. & Suwanboon, S. 2012. Photocatalytic and antibacterial activities of Ag-doped ZnO thin films prepared by a sol–gel dip-coating method. *Journal of Sol-Gel Science and Technology* 62: 304–312.

Wang, Q., Gang, B.Y. & Wang, S.Z. 2009. ZnO/Au hybrid nanoarchitectures: Wet-chemical synthesis and structurally enhanced photocatalytic performance. *Environmental Science & Technology* 43: 8968–8973.

Xia, S.J., Zhang, L.Y., Zhou, X.B., Shao, M.M., Pan, G.X. & Ni, Z.M. 2015. Fabrication of highly dispersed Ti/ZnO–Cr_2O_3 composite as highly efficient photocatalyst for naphthalene degradation. *Applied Catalysis B: Environmental* 176: 266–277.

Yang, Y.B., Li, Z., Zhao, W., Zhao, C.X., Wang, Y. & Liu, X.Q. 2014. Controllable synthesis of Ag–CuO composite nanosheets with enhanced photocatalytic property. *Materials Letters* 120: 16–19.

Zhang, Y.J., Wang, Y.C., Yan, W., Li, T, Li, S. & HU, Y.R. 2009. Synthesis of Cr_2O_3/TNTs nanocomposite and its photocatalytic hydrogen generation under visible light irradiation. *Applied Surface Science* 255: 9508–9511.

Sze-Mun Lam*
Department of Environmental Engineering
Faculty of Engineering and Green Technology
Universiti Tunku Abdul Rahman
Jalan Universiti, Bandar Barat
31900 Kampar, Perak Darul Ridzuan
Malaysia

Jin-Chung Sin
Department of Petrochemical Engineering
Faculty of Engineering and Green Technology
Universiti Tunku Abdul Rahman
Jalan Universiti, Bandar Barat
31900 Kampar, Perak Darul Ridzuan
Malaysia

Abdul Rahman Mohamed
School of Chemical Engineering
Universiti Sains Malaysia
Engineering Campus
Seri Ampangan, 14300 Nibong Tebal, Pulau Pinang
Malaysia

*Corresponding author; email: lamsm@utar.edu.my

Received: 25 March 2017
Accepted: 1 August 2017